Analysis of Selected Data from the Triservice Missile Data Base

Jerry M. Allen,* David S. Shaw,† and Wallace C. Sawyer‡
NASA Langley Research Center, Hampton, Virgina

A large, systematic, axisymmetric-body/tail-fin data base has been gathered through tests of an innovative missile model design that is described in this paper. These data were originally obtained for incorporation into a missile aerodynamics code based on engineering methods (program MISSILE3), but these data are also valuable as diagnostic test cases for developing computational methods because of the individual-fin data included in the data base. Detailed analyses of four sample cases from these data are presented to illustrate interesting individual-fin force and moment trends. These samples quantitatively show how bow shock, fin orientation, fin deflection, and body vortices can produce strong, unusual, and computationally challenging effects on individual fin loads. Flow-visualization photographs are examined to provide physical insight into the cause of these effects. It was found that body vortices had a strong influence on the fin loads and that large fin deflections could induce loads on adjacent fins.

Nomenclature

$\mathcal{R}$	= fin aspect ratio
C_{HM}	= fin hinge moment coefficient, fin hinge moment/$(q_\infty * CR * SF)$
C_N	= model normal-force coefficient; normal force/$(q_\infty * SB)$
C_{NF}	= fin normal-force coefficient, fin normal force/$(q_\infty * SF)$
CR	= fin root chord
L	= body length
M_∞	= freestream Mach number
q_∞	= freestream dynamic pressure
SB	= body cross-sectional area
SF	= fin planform area
TR	= fin taper ratio
Z	= axial coordinate measured from body nose
α	= model angle of attack
δ	= fin-deflection angle
ϕ	= model roll angle measured from windward meridian
$\partial C_{NF}/\partial\delta$	= fin-control effectiveness parameter

Introduction

In the early 1980s, NASA Langley entered into a cooperative agreement with the three service branches of the U.S. Department of Defense and with industry (Nielsen Engineering and Research, Inc.) to develop a systematic, high-quality, body/tail-fin force and moment data base to be used in high-angle-of-attack missile aerodynamics computer programs based on engineering methods, specifically, program MISSILE3.[1] The objective of this cooperative program is shown in Fig. 1. Since an extremely large body of data was needed for this task, a unique model was designed and constructed to allow this quantity of data to be obtained in a reasonable time frame. The model has been named the Langley Remote Control Missile Model. The inset in Fig. 1 illustrates the envelope of fin data that was needed in the MISSILE3 code compared to that which existed prior to this program. The data set defined by this envelope has been termed the Triservice Missile Data Base.

All three branches of the U.S. Department of Defense—Army, Navy, and Air Force—participated in the funding of this project. Nielsen Engineering and Research, Inc., designed the fins and organized the data in the form of a data base and incorporated these data into a high-angle-of-attack engineering prediction method that they had developed. Preliminary versions of this engineering code were called programs MISSILEl,[2] MISSILE2,[3] and MISSILE2A.[4] NASA Langley modified an existing remote control missile model to accept the fin balances necessary for this project, designed and fabricated the three-component fin balances, provided the wind-tunnel facilities and testing time, conducted the wind-tunnel tests, and analyzed the data.

This paper is organized in the following manner. A description of the Remote Control Missile Model is presented first, followed by a review of the wind-tunnel tests that were conducted to gather the data. Selected examples from these data are then analyzed to highlight some of the interesting data trends that were discovered because of the unique features of this model. Data are analyzed in the following categories: 1) bow shock wave from the body interacting with the fins, 2) fin-control effectiveness over the range of model roll orientations, 3) fin-on-fin interference for a deflected fin, and 4) body vortex interference on fins. Vapor-screen photographs of these selected cases will be examined as an aid to understanding the flow phenomenon.

Presented as Paper 89-0478 at the AIAA 27th Aerospace Sciences Meeting, Reno, NV, Jan. 9-12, 1989; received Jan. 26, 1989; revision received May 10, 1989. Copyright © 1989 American Institute of Aeronautics and Astronautics, Inc. All rights reserved. No copyright is asserted in the United States under Title 17, U.S. Code. The U.S. Government has a royalty-free license to exercise all rights under the copyright claimed herein for Governmental purposes. All other rights are reserved by the copyright owner.

*Aero-Space Technologist, Supersonic/Hypersonic Aerodynamics Branch, Applied Aerodynamics Division. Associate Fellow AIAA.

†Aero-Space Technologist, Supersonic/Hypersonic Aerodynamics Branch, Applied Aerodynamics Division. Member AIAA.

‡Assistant Chief, Advanced Vehicles Division. Associate Fellow AIAA.

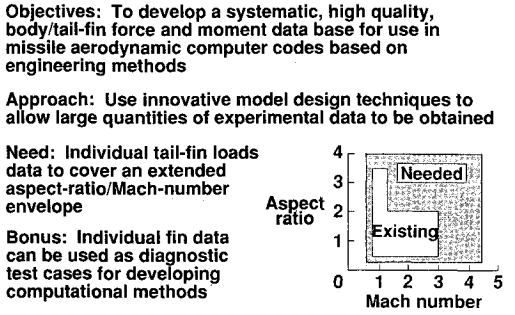

Fig. 1 Introduction.

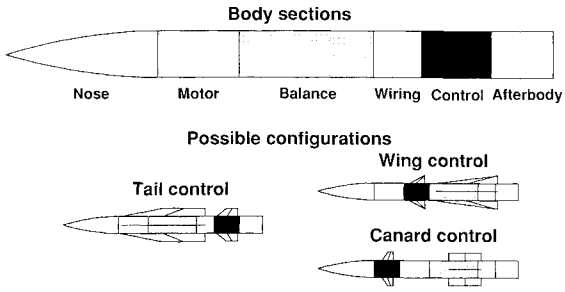

Fig. 2 Remote-control missile model.

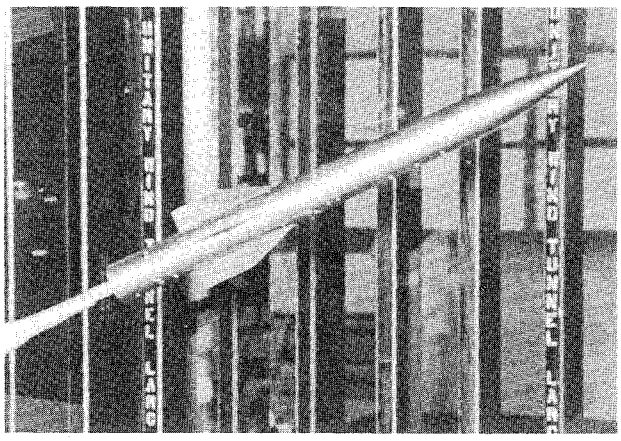

Fig. 3 Triservice missile photograph.

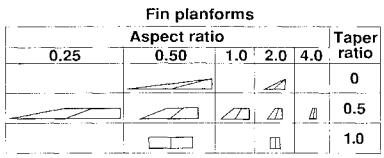

Fig. 4 Fin planforms.

Model Description

The missile model body used in this project, shown schematically in the top part of Fig. 2, is about 12.3 calibers in length with a 3-caliber tangent ogive nose. As shown in the figure, the body is composed of six separate sections, with each section serving a separate and unique function. The nose section contains an internal roll mechanism that rotates the entire model about the main balance, which remains at a fixed orientation. This roll mechanism serves two purposes: 1) it simplifies the main balance data reduction process since the balance always remains upright, and 2) it allows this model to be tested in wind tunnels that do not have model roll capability. The motor section contains the four drive motors for the remote control fins. The balance section houses the main balance that measured the overall loads on the model. Located along this section are longitudinal slots for mounting fins. The wiring section contains harnesses for connecting the electrical wiring for the motors and fin balances and for routing these wires down the inside of the sting. The control section contains the mounting arrangements for the remotely deflectable fins, which are operated through drive shafts from the motor section. The afterbody is the only section that did not contain hardware necessary for the operation of this model. It should be emphasized that, with the exception of the nose and afterbody sections, each section of this model is interchangeable, so that the remote-control fins can be mounted at various locations along the body length. This is illustrated in the bottom part of Fig. 2, in which typical canard-control, tail-control, and wing-control configurations are pictured.

Because only body/tail-fin data were needed for this project, the full capabilities of this model for providing interchangeable fin locations were not used. The photograph in Fig. 3 shows a typical configuration employed in this project. The key features of this model are the remote-control fins, the internal roll capability, interchangeable fin locations, and the ability to measure individual-fin loads. Once a set of fins has been installed on this model, all attitude parameters (angle of attack, roll angle, and fin-deflection angle) could be changed during testing without interrupting the wind-tunnel operation. Thus, this Triservice configuration offered the potential of obtaining the large quantity of body/tail-fin data required for this project.

As shown in Fig. 4, nine sets of cruciform fins were designed and constructed for this project. The fin planforms were selected to provide a wide and systematic variation of aspect and taper ratios. As seen in the sketches, the fins varied in aspect ratio from 1/4 to 4 and in taper ratio from 0 to 1. All fins have a semispan equal to the body radius.

The five fins shown on the right in Fig. 4 ($AR \geq 1.0$) are movable and designed to be mounted on the control section of the body. The remaining four fins are designed to mount in the slots in the balance section of the body and are not movable. They have their own fin balances, however.

All of the Triservice missile tests were conducted with single sets of cruciform fins located as tail fins near the base of the model, as illustrated by the model photograph in Fig. 3. Selected data from three of these fins are analyzed in this paper.

Description of Tests

The-low-Mach-number tests (Mach numbers of 2.0 or smaller) were conducted in the NASA Ames 6×6 wind tunnel, whereas the high-Mach-number tests (Mach numbers of 2.5 or greater) were conducted in the NASA Langley Unitary Plan wind tunnel (test section 2). Because of the volume of data gathered, these tests required multiple tunnel entries over a 5-yr period ending in 1985.

The model angle of attack for these tests ranged from about -5 to 45 deg in 5-deg increments, the roll angle ranged through 180 deg in 10-deg increments, and the fin-deflection angle of the control fins ranged from -40 to $+40$ deg in 10-deg increments. Fins were always mounted in a cruciform arrangement. For the fin-deflection tests all four fins were present, but only one fin was deflected. Fin loads were measured for all four fins.

Over 60,000 individual data points were recorded in this project, with each point containing 25 measured quantities. This resulted in a total of approximately 1.5 million quantities measured in this program. All data were recorded on magnetic tape. The data base needed for program MISSILE3 has been compiled and incorporated into the code. References 5 and 6 contain analyses of missile configurations using the MISSILE3 code. References 7–11 contain aerodynamic studies that use parts of the Triservice data base. Publication of the complete tabulated data base is currently underway at NASA Langley.

Analysis of Selected Data

During the acquisition and preliminary analysis of these data, many interesting patterns were observed in the individual fin data. Four of these cases have been selected for analysis and presentation in this paper. A subsequent wind-tunnel entry into Langley's Unitary Plan wind tunnel was made to obtain vapor screen photographs of the flowfield patterns for these cases. These flow-visualization data provided invaluable information to assist in interpreting the trends observed in the force and moment data.

Body Shock-Wave/Fin Interaction

The first case involves the effects of a fin being intersected by the body bow shock wave. As shown in Fig. 5, the configuration analyzed is the body with the $AR = 0.25/TR = 0.5$ fin. Since this is one of the fixed fins, no fin deflections were involved. The data shown is for Mach 2.0 and 4.5 at angles of attack from 20 to 40 deg. Fin data are shown as the fin rolls from windward to leeward, as indicated in the cross-sectional sketch in this figure. In the sketch the solid line represents the fin that is providing the data in subsequent figures. The dashed lines for the other three fins indicate that these fins were present on the body during testing, but that their data are not being presented.

At the lower supersonic Mach number, the bow shock does not intersect the fin even at the highest angle of attack. As the Mach number increases to 4.5, the bow shock intersects the windward fin at the highest angle of attack, as illustrated by the model sketch in this figure. Thus, if any effect of this shock wave on the fin is present, it will occur at the highest Mach number and the highest angle of attack.

Fin normal-force and hinge moment coefficients for this case are shown in Fig. 6. The small cross-sectional sketch in this figure indicates the positive directions of the normal force and roll angle. The hinge moment shown at the bottom of this figure is essentially the pitching moment of the fin about its hinge line. For these fins this hinge line is located at about the midpoint of the root chord. Hence, the negative hinge moments shown in this figure together with the positive normal forces indicate that the center of the normal force is located downstream of the hinge line, causing a leading-edge-down moment.

The normal-force trends for all conditions, seen at the top of this figure, are smooth and reasonable with the expected zero normal force on both the leeward and windward meridians. As the roll angle increases, the normal force increases and reaches a maximum at about 60 deg from the windward meridian and decreases thereafter. The negative normal force near the leeward meridian in some cases will be examined in a subsequent section of this paper. The normal force increases with angle of attack, as would be expected; however, note that the maximum force at each angle of attack does not occur in the horizontal plane but at about 30 deg windward from this plane.

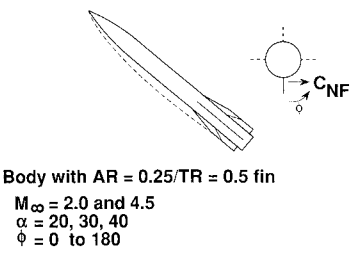

Fig. 5 Schematic of bow-shock/fin interaction.

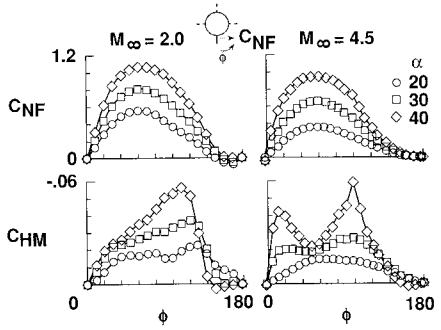

Fig. 6 Effect of bow-shock interaction on fin loads. $AR = 0.25/TR = 0.5$ fin.

Corresponding hinge moment data are shown at the bottom of Fig. 6. Fin hinge moment is essentially the pitching moment of the individual fin about its hinge line, which for this fin is located at about the 55% root chord station. The trends again appear reasonable for the Mach 2.0 data, with the maximum hinge moment occurring about 30 deg leeward from the horizontal plane. However, the hinge moment data at Mach 4.5 show an irregular variation at the highest angle of attack. Two unusual aspects of these data are evident. The first aspect is the sharp negative peaks that occur near the windward meridian and just leeward of the horizontal plane. Since positive hinge moment refers to a tendency to bend the leading edge upward, these negative peaks indicate a sharp rearward movement of the aerodynamic center of the fin in a region where there is smoothly varying normal force. The second aspect is the minimum in hinge moment that occurs in the region just windward of the horizontal plane. Note that this is the region where the fin normal force reaches a maximum.

Figure 7 shows schlieren photographs to illustrate the bow shock-wave patterns for this case. The photographs on the left in this figure are for a slightly higher Mach number than was shown in the previous figure because schlierens at the lower Mach number were not available. Also, the fact that different fins are shown in these photographs does not affect the bow shock location comparisons since all fins in this project had the same semispan. These photographs confirm that only at the highest Mach number and angle of attack does the bow shock intersect the lower fin. This intersection is also confirmed by vapor screen photographs in Fig. 8.

Fin-Control Effectiveness

The next data trend examined is the effectiveness of control fin deflections as the fin is rolled from the most windward to the most leeward position. In this case, the missile configuration and test conditions consist of the following: body with the $AR = 2.0/TR = 0.5$ fin, Mach 2.0 and 4.5, 20-deg angle of attack, and fin-deflection angles of -40 to $+40$ deg.

The effects of fin-deflection angle and roll angle on fin normal force are presented in Fig. 9. Positive deflection means leading edge upward. Positive deflection thus increases the ef-

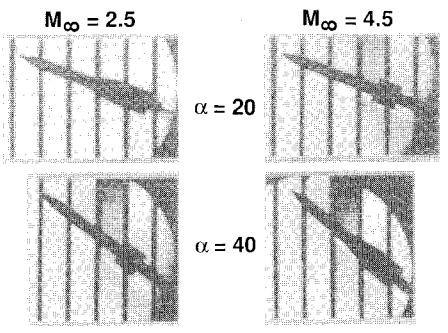

Fig. 7 Effect of Mach number on bow-shock location.

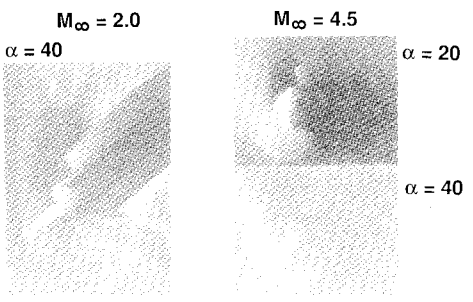

Fig. 8 Effect of Mach number on shock-wave patterns; $AR = 0.25/TR = 0.5$ fin, $\phi = 0$, $\delta = 0$, $Z/L \approx 0.9$.

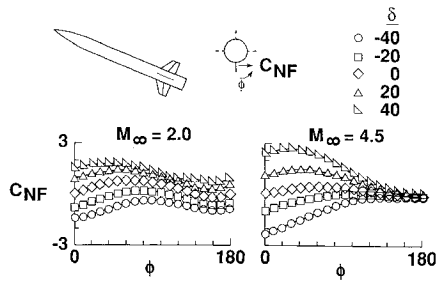

Fig. 9 Effect of fin orientation on fin loads; $\mathcal{R}=2.0/TR=0.5$ fin, $\alpha=20$.

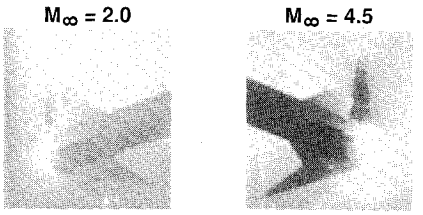

Fig. 10 Effect of Mach number on body vortices; $\mathcal{R}=2.0/TR=0.5$ fin, $\alpha=20$, $\phi=0$, $\delta=0$, $Z/L\approx0.9$.

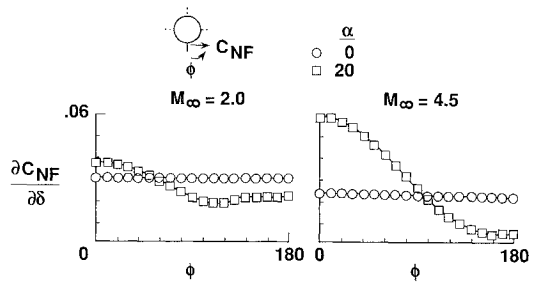

Fig. 11 Fin-control effectiveness; $\mathcal{R}=2.0/TR=0.5$ fin.

fective angle of attack of the fin, which increases the fin normal force at all roll angles, as would be expected. At the lower Mach number, the normal force on the fin experiences only a small change as the fin is rolled from windward to leeward. However, a steady decrease in the effect of fin deflections with roll angle occurs at the higher Mach number. On most of the leeward side of the body at this Mach number the fin-control authority essentially disappears. An often-observed trend in missile aerodynamics is that fins become ineffective when shielded from the freestream flow at high Mach numbers. These data clearly show that this loss of control authority results from the very small forces on the leeward fins.

Figure 10 shows vapor screen photographs for this case. Note that at the lower Mach number a pair of well-defined body vortices are present. At the higher Mach number, however, these vortices have merged into one large shadow region. It is within this region that fin effectiveness is virtually eliminated.

The parameter $\partial C_{NF}/\partial\delta$, calculated from these data, is shown in Fig. 11 for angles of attack of 0 and 20 deg. The 0-deg angle-of-attack results, of course, contain no effect of roll angle at either Mach number; however, the fin effectiveness is slightly larger at the lower Mach number. At the higher Mach number, there is a very large fin effectiveness near the windward meridian and a large variation of control authority with fin orientation compared to the lower Mach number results. This figure shows quantitatively the almost complete lack of control authority on the leeward side of the body at the higher Mach number.

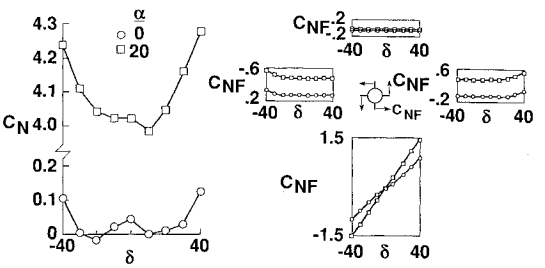

Fig. 12 Fin-on-fin interference for windward fin deflection; $\mathcal{R}=1.0/TR=0.5$ fin, $M_\infty=3.0$, $\phi=0$.

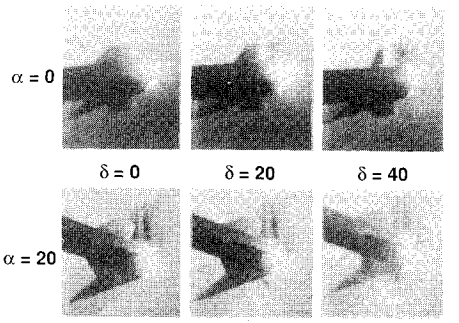

Fig. 13 Effect of fin deflection on fin shock-wave patterns; $\mathcal{R}=1.0/TR=0.5$ fin, $M_\infty=3.0$, $\phi=0$, $Z/L\approx0.9$.

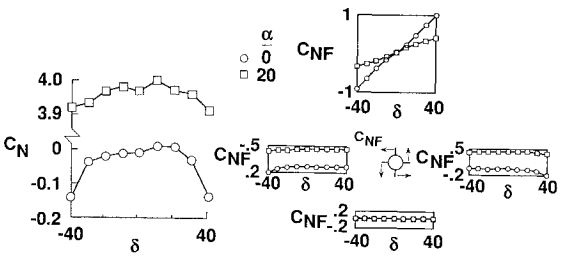

Fig. 14 Fin-on-fin interference for leeward fin deflection; $\mathcal{R}=1.0/TR=0.5$ fin, $M_\infty=3.0$, $\phi=180$.

Fin-Deflection Interference

The next case examined is the interference that can occur between a highly deflected fin and the other three fins when all four fins are placed in a cruciform arrangement. As seen in Fig. 12, these results are for the body with the $\mathcal{R}=1.0/TR=0.5$ fin, Mach 3.0, angles of attack of 0 and 20 deg, and fin-deflection angles from -40 to $+40$ deg. The effects of fin deflection on both the overall missile normal force and the individual-fin normal forces are examined.

This figure presents these data at both 0- and 20-deg angle of attack with only the lower fin deflected. The small data plots near each fin in the sketch show the resulting normal force on that fin. At the left in this figure, a noticeable increase in normal force occurs on the model at both angles of attack when the fin-deflection angle becomes very large, both positive and negative. Since the lower fin, even when deflected, is in the vertical plane, the normal force on that fin could not contain an upward component. Thus, the increase in the normal force on the model is not caused by the force acting on the deflected fin.

Examining the forces on the individual fins in this case reveals a very interesting pattern. The lower (deflected) fin naturally shows a very large and systematic variation of normal force with deflection angle. Remember that fin normal force is always normal to the plane of the fin regardless of its angular orientation.

At zero angle of attack very small fin forces would be expected to occur on the undeflected fins. The top fin indeed shows very little force. The horizontal fins also show very little force for the small deflection angles. However, for the larger deflection angles, a noticeable normal force occurs on these fins but not at the same time. The force on the right fin increases for large positive deflection angles, and, conversely, the force on the left fin increases for large negative deflection angles. In either case, the force increases on the fin that is nearest to the trailing edge of the deflected fin. The level of the induced forces on the horizontal fins, when converted to overall normal force form, is about the same magnitude as the induced model normal forces shown on the left side of this figure. Thus, the increased normal force on the missile results from induced forces on the horizontal fins.

Figure 13 shows vapor screens for this case. At both angles of attack, fin deflections cause the shock wave emanating from the fin to become both larger and stronger. The strongest area of this shock wave appears to occur on the side of the body nearest to the trailing edge of the deflected fin. Also, the increased size of this shock at the largest deflection angle causes it to overlap onto the adjacent fins. The fin interference effects noted in the force data thus appear to be caused by the enlarging and strengthening of the shock wave on the compression side of the deflected fin.

Figure 14 shows results similar to those of Fig. 12, except that the top fin is deflected instead of the bottom fin. At zero angle of attack a trend very similar to that shown for the bottom fin in Fig. 12 occurs, except that all of the induced forces are downward, as expected. When the leeward fin is deflected to 20-deg angle of attack, the induced forces virtually disappear. Note also that the forces on the deflected fin are also much less than those for the windward case due to the body-shielding effect discussed earlier.

In reviewing these results, it can be concluded that a large deflection of both windward and leeward fins in the same direction should produce very little induced rolling moment on the configuration at zero angle of attack. This occurs because the induced forces on the horizontal fins are approximately equal but are in opposing directions and cancel each other. However, at 20-deg angle of attack the deflected fins not only create a rolling moment but also induce an additional rolling moment on the horizontal fins.

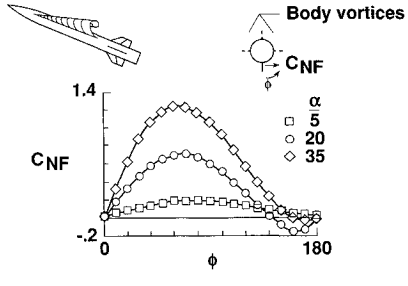

Fig. 15 Effect of angle of attack on fin force reversal; $\mathcal{R}=1.0/TR=0.5$ fin, $M_\infty=2.0$, $\delta=0$.

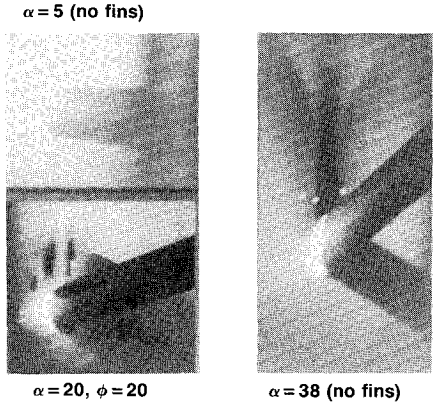

Fig. 16 Effect of angle of attack on body vortices; $\mathcal{R}=1.0/TR=0.5$ fin, $M_\infty=2.0$, $\delta=0$, $Z/L\approx0.9$.

Body-Vortex/Fin Interference

The last data pattern analyzed in this paper is the effect of body vortices on fin loads. As shown in the model sketch in Fig. 15, vortices that develop on the body are located, for certain flow conditions, in a position to directly influence the loads on fins on the leeward side of the missile. The individual-fin data from this program permit this phenomenon to be investigated. Shown in this figure are fin normal-force data for the body with the $\mathcal{R}=1.0/TR=0.5$ fin at Mach 2.0 at low to high angles of attack with no fin deflections. Fin normal force is shown as the fin is rolled from windward to leeward.

The vortex pattern shown in this figure was sketched from a vapor screen photograph taken near the downstream end of this model at about 20-deg angle of attack. At this angle, the body vortices are located in a position to pass directly over the fins on the leeward side of the body. Notice that the expected trend with roll angle is observed until the fin approaches the leeward meridian; here the normal force becomes negative in the region of about 40 deg from leeward, with the largest negative value occurring at about 20 deg from the leeward meridian. With the sign convention used in this paper, this means that the force on the fin is actually in the downward direction even though the configuration is at 20-deg angle of attack. It should be emphasized that no fin deflections are involved here. This force reversal does not occur at either the low or high angles of attack, 5 and 35 deg, respectively.

Figure 16 shows vapor screen photographs for this case. At the lower angle no vortices appear on the vapor screens. At the moderate angle, two distinct body vortices are seen. At the highest angle, these vortices have merged into one elongated shadow region. The fin force reversal seen in Fig. 15 occurred only at the moderate angle, where the distinct vortices appear. Note that the shadow region at the highest angle of attack appears similar to that seen in Fig. 10 at Mach 4.5 at 20-deg angle of attack. In both instances, when the body vortices merged into a single shadow region, very small loads were measured on the fin in the shadow region.

Figure 17 shows that this force reversal is still present at Mach 2.0 when the angle of attack is reduced to 10 deg. How-

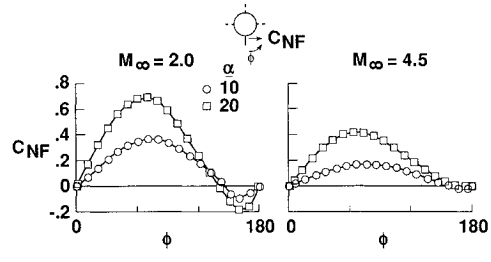

Fig. 17 Effect of Mach number on fin force reversal; $\mathcal{R}=1.0/TR=0.5$ fin, $\delta=0$.

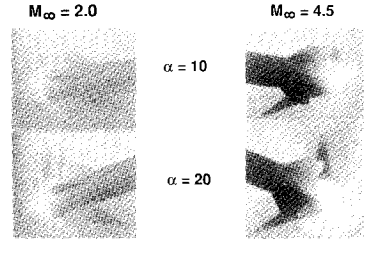

Fig. 18 Effect of Mach number and angle of attack on body vortices; $\mathcal{R}=1.0/TR=0.5$ fin, $\phi=20$, $\delta=0$, $Z/L\approx0.9$.

ever, this reversal effect is noticeably reduced at Mach 4.5 and 10-deg angle of attack and vanishes entirely at 20-deg angle of attack.

Figure 18 shows comparisons of the vapor screens at the low and high Mach numbers at 10- and 20-deg angle of attack. At the lower Mach number, as the angle of attack is reduced from 20 deg to 10 deg, the vortices become smaller and result in the reduced fin force reversal effect seen in the previous figure. This effect is not present at Mach 4.5 and 20-deg angle of attack due to the merged vortices. At 10 deg a very small force reversal occurs, and the vapor screens show that the body vortices have not yet merged. Note, however that these vortices have not lifted off the body surface.

Conclusions

An extremely large, systematic, axisymmetric-body/tail-fin data base has been gathered through tests of a missile model featuring remotely controlled fins. A detailed analysis of four sample cases from this data base is presented to illustrate interesting individual-fin force and moment trends. Flow-visualization photographs are used to enhance the analysis of these trends. These samples quantitatively show how bow shock, fin orientation, fin deflection, and body vortices can produce strong, unusual, and computationally challenging effects on individual-fin loads. Based on these results the following conclusions have been drawn:

1) Large moments were found on fins that were being intersected by the body bow shock wave.

2) At high Mach numbers and/or angles of attack, individual body vortices merged into a single elongated shadow region where fin-control effectivenesss was virtually eliminated.

3) Large fin-deflection angles altered the loads on adjacent undeflected fins on the trailing edge side of the deflected fin.

4) Body vortices caused reversals in the direction of fin forces on the leeward side of the body.

References

[1]Lesieutre, D. J., Mendenhall, M. R., Nazario, S. M., and Hemsch, M. J., "Prediction of Aerodynamic Characteristics of Cruciform Missiles Including Effects of Roll Angle and Control Deflection," Nielsen Engineering and Research, Inc., Mountain View, CA, TR-360, Aug. 1986.

[2]Nielsen, J. N., Hemsch, M.J., and Smith, C. A., "A Preliminary Method for Calculating the Aerodynamic Characteristics of Cruciform Missiles to High Angles of Attack Including Effects of Roll Angle and Control Deflections," Nielsen Engineering and Research, Inc., Mountain View, CA, TR-152, Nov. 1977.

[3]Smith, C. A., and Nielsen, J. N., "Prediction of Aerodynamic Characteristics of Cruciform Missiles to High Angles of Attack Utilizing a Distributed Vortex Wake," Nielsen Engineering and Research, Inc., Mountain View, CA, TR-208, Jan. 1980.

[4]Hemsch, M. J., and Mullen, J., Jr., "Analytical Extension of the MISSILEl and MISSILE2 Computer Programs," Nielsen Engineering and Research, Inc., Mountain View, CA, TR-272, March 1982.

[5]Lesieutre, D. J., Mendenhall, M. R., Nazario, S.M., and Hemsch, M. J., "Aerodynamic Characteristics of Cruciform Missiles at High Angles of Attack," AIAA Paper 87-0212, Jan. 1987

[6]Lesieutre, D. J., Mendenhall, M. R., and Dillenius, M. F. E., "Prediction of Induced Roll on Conventional Missiles with Cruciform Fin Sections," AIAA Paper 88-0529, Jan. 1988.

[7]Nielsen, J. N., Goodwin, F. K., Dillenius, M. F. E., and Hemsch, M. J., "Prediction of Cruciform All-Movable Control Characteristics at Transonic Speeds," AIAA Paper 84-0312, Jan. 1984.

[8]Hemsch. M. J., and Nielsen, J. N., "Extension of Equivalent Angle-of-Attack Method for Nonlinear Flowfields," *Journal of Spacecraft and Rockets,* Vol. 22, May-June 1985, pp. 304-308.

[9]Hemsch, M. J., "Nonlinear Applications of Slender-Body Theory to Missile Aerodynamics," AIAA Paper 85-1775, Aug. 1985.

[10]Nielsen, J. N., "Supersonic Wing-Body Interference at High Angles of Attack with Emphasis on Low Aspect Ratios," AIAA Paper 86-0568, Jan. 1986.

[11]Allen, J. M., Shaw, D. S., and Sawyer, W. C., "Remote Control Missile Model Test," *Stability and Control of Tactical Missile Systems*, AGARD CP-451, March 1989, pp. 17-1 to 17-2.

Watch for our special issue on . . .

COMPUTATIONAL FLUID DYNAMICS

The March-April 1990 issue of the **Journal of Spacecraft and Rockets** will be devoted exclusively to the topic of Computational Fluid Dynamics.

If you're not already a subscriber, you can subscribe now and get this special issue **plus** the rest of the year!

Subscribe Today!

1990 Rates	North America	Outside North America*
Nonmembers	$155	$185
AIAA Members	25	40

*Now includes automatic airmail delivery!

AIAA

American Institute of Aeronautics and Astronautics
370 L'Enfant Promenade, S.W. Washington, DC 20024-2518

Phone: (202) 646-7400